Advanced Interface Concepts for Rollable Composite Space Booms under Test in Artificial Weightlessness

Marco Straubel* and Martin Hillebrandt†
DLR Institute of Lightweight Systems, Braunschweig, Germany

In July 2021, DLR conducted a test campaign in artificial weightlessness. During a dedicated flight day, the entire 20 m x 5 m test area of the special Airbus A310 was available for 5 experiments in the field of deployable high strain composite space structures. The results presented here originate from experiment No4 in which two different deployment mechanisms for DLR's deployable CFRP masts were tested. Both types of mechanisms use new interface concepts to attach the booms to the satellite structure with high stiffness during and after deployment. Both concepts were extensively evaluated in artificial weightlessness with respect to their safe deployment and stowage as well as their resulting interface stiffness. For this purpose, the test setup in the aircraft, the test plan and the test procedure are described. Finally, the results are discussed and recommendations are given for the further development of the boom and mechanisms as well as the testing of such structures in artificial weightlessness.

I. Nomenclature

a_x	=	longitudinal acceleration within the aircraft
a_y	=	lateral acceleration within the aircraft
a_z	=	vertical acceleration within the aircraft
E	=	elastic modulus
F	=	force
f_A	=	vibration decay frequency of *Concept A*
$f_{A\|CamX}$	=	vibration decay frequency of *Concept A* obtained with camera #X
$f_{B\|weak\|Mx}$	=	vibration decay frequency of *Concept B* with undeployed boom root oscillating around boom x-axis
$f_{B\|weak\|My}$	=	vibration decay frequency of *Concept B* with undeployed boom root oscillating around boom y-axis
$f_{B\|stiff\|Mx}$	=	vibration decay frequency of *Concept B* with deployed boom root oscillating around boom x-axis
$f_{B\|stiff\|My}$	=	vibration decay frequency of *Concept B* with deployed boom root oscillating around boom y-axis
g	=	$9.81 m/s^2$
I	=	geometrical moment of inertia
M	=	bending torque
n_{decay}	=	number of observed full oscillations
$T_{decay,n}$	=	vibration decay period for n_{decay} full oscillations

II. Introduction

The DLR Institute of Lightweight Systems[‡] has developed a large number of concepts for deployable space structures for versatile applications[1]. All of them rely on high strain composites. The majority of the concept uses DLR's rollable CFRP masts (see Fig. 1) and dedicated deployment control mechanisms developed, built and tested in-house.

A. Motivation

The mast design, sizing, analysis and manufacturing has been researched for decades and have reached a high level of technical maturity. However, the more the understanding of the booms themselves grew, the clearer it became that the

*Space Structures and Mechanisms Engineer, Composite Design Department, Marco.Straubel@dlr.de
†Space Structures and Mechanisms Engineer, Composite Design Department, Martin.Hillebrandt@dlr.de
‡former DLR Institute of Composite Structures and Adaptive Systems, renamed in 2023

Fig. 1 DLR's rollable CFRP booms in different cross section variations.

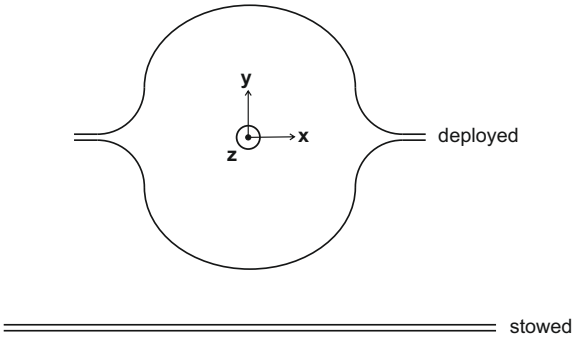

Fig. 2 Boom cross sections in deployed and stowed state with reference coordinate system definition

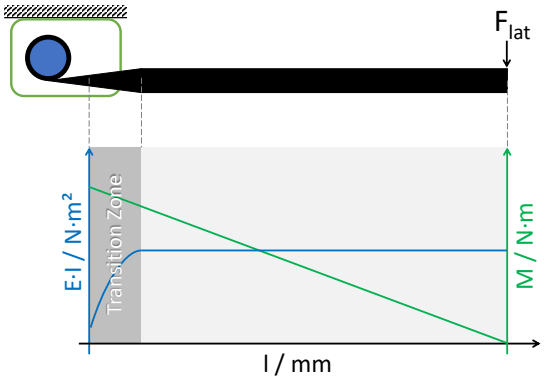

Fig. 3 Visualization of coinciding positions of weakened transition zone and highest bending load

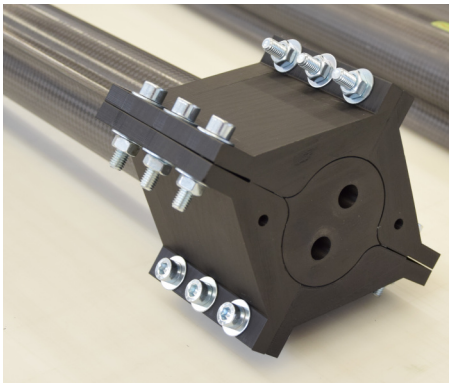

Fig. 4 Ideal, solid boom interface for laboratory stiffness testing

performance of each perfectly tuned boom could easily be reduced by a factor of 2 or more if the interfaces between boom and satellite were poorly chosen.

This is primarily effecting the local bending stiffness and strength around the x-axis (see axis definition in Fig. 2). As secondary effects of this local reductions, the global stability and stiffness is reduced as well.

B. Understanding the Key-Issue

The reason for this severe knock-down factors is visualized in Fig. 3. The upper part of the figure shows a schematic boom deployment mechanism (green) attached to the carrying spacecraft, a boom (black) and the boom spool (blue). The lower part of the figure shows the approximated curves of the bending stiffness EI around the booms x-axis (blue graph) and a bending torque M resulting from a generic laterally acting load F_{lat} (load in y-direction, bending moment around x-axis, green graph). The critical region along a partially or fully deployed and loaded boom is the so-called *transition zone* which marks the section of the boom where it is no longer coiled onto the boom spool but the cross section has also not fully opened up.

The bending stiffness in the *transition zone* is significantly decreased. Furthermore, the bending torque M reaches its maximum at the point of maximum distance to the causing lateral load. Consequently, the highest bending load on the mast is generated at the weakest section of it.

This weak interface between boom and spacecraft also generates drawbacks for global column buckling resulting from compression or combined compression and bending loads. To understand this weakening one need to understand that the decrease in *bending stiffness* EI is solely resulting from the cross-section depending *geometrical moment of inertia* I. The relation between the level of cross-section deployment and I is highly non-linear.

Additionally, the bending strength in this zone is also decreased as a combination of higher tension in the compression-

loaded boom shell due to reduced distance between this shell and the neutral fiber and the lower buckling load of the compression-loaded shell due to the wider cross section with resulting increased cross section contour radii. Even worse, when loaded with a too high lateral load the booms cross section tends to flatten itself and can even collapse fully.

C. Approach

Interfacing a boom without the negative effects of a transition zone is only possible under laboratory conditions with stiff, custom-built clamping blocks (see Fig. 4). Since the booms deform their cross-section during deployment, such clamping blocks cannot be used in combination with deployment mechanisms.

The only known concept that could use pretty solid interfaces at are so called *tip-deployment concepts*. These concepts fix the free tip of the boom to the spacecraft and use a mobile deployment unit that is moving away from the spacecraft while deploying the boom. This leads to a high tip mass due to the deployment mechanisms at the tip but could - when combined with a jettison-functionality - result in an very light, deployed structure. The resulting debris creation wouldn't be acceptable for usual Earth orbits but could be applicable to interplanetary mission with high demands in mass reduction for example to increase the acceleration resulting from a given electric propulsion system. More detailed thoughts on that are described by Straubel et al. in [2].

Away from such concepts, it must be acknowledged that it will be difficult to design a mast support for the mast outlet of a deployment mechanism that offers a similar performance as the ideal interface does. In the following, two concepts are presented that seek to come close to this optimum. Both concepts were tested in a parabolic flight in summer 2021. The focus of these tests lay on functional tests to show that all important sub-mechanisms operate properly in weightlessness. In addition, vibration decay tests were carried out which allow insight in the achieved stiffness via the evaluation of the oscillation frequency.

III. Advanced Boom Root Interfaces

The following section introduce the two most advanced boom root interface concepts. Core concepts of both systems are protected by already granted [3] or applied patents [4].

A. Concept A - The Floating Core

Concept A supports the boom transition zone by a combination of two outer guiding half-shells and one inner core (see Fig. 5). There is only a small gap between the shells and the core through which the boom can pass when extending and stowing. The concept is described to more detail in a dedicated paper of Hillebrandt et al. [5].

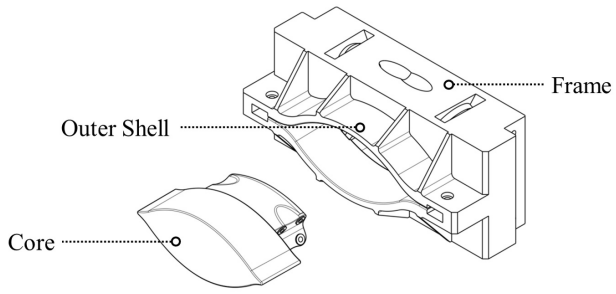

(a) Visualization of the floating core principle used for *Concept A* [6]

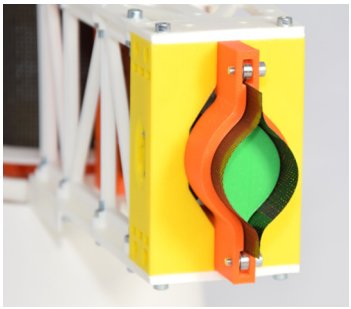

(b) Detailed view on a *Concept A* demonstrator showing the Floating Core (green), the outer shells (orange) and short piece of boom (black) sticking out

Fig. 5 Details on *Concept A*

B. Concept B - The Deploying Root

In contrast, *Concept B* is not trying to support the boom in its transition zone but is avoiding the existence of such zone. It uses an additional mechanism inside the boom spool to fully open up the boom cross section at the end of the longitudinal boom deployment. This results in a very advanced stiffness and strength behaviour for a fully

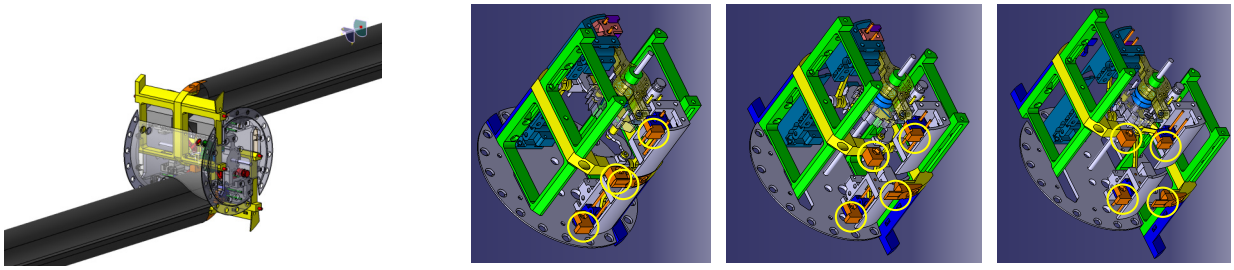

(a) A single boom spool implementing *Concept B* for a two-boom deployment mechanism.

(b) Inner boom spool deployment sequence of *Concept B* for fully stowed (left), partially deployed (middle) and fully deployed (right) configuration

Fig. 6 Details on *Concept B*

deployed boom but also limits the possibilities for a good boom support during deployment. Thus this concept is suited for applications that do not required high loads during deployment but required high mechanical performance once deployed.

The basic principle of *Concept B* is relying on two main-functions that are realized in a integrated approach:

I: Deploying the boom root (the segment of the boom that is directly connected to the boom spool) by a boom spool integrated mechanisms

II: Locking the boom spool into the sidewalls of the mechanisms housing to prevent further rotation of the boom spool and thereby a pivoting of the boom that is then fixed to the boom spool

Fig. 6a shows such a boom spool with integrated mechanism in deployed state. This spool can carry up to two booms that are deployed with 180° angular offset. Fig. 6b briefly introduces the inner mechanism installed in the spool. The three sub-figures show 3 different stages of deployment. The four yellow circles mark the boom interface brackets (orange) that are the only parts that are in contact to the boom. Those brackets are attached to the boom spool by screws. The brackets are attached to the boom by an appropriate adhesive aided by a dedicated rig.

During the unfolding process of the boom root, these interface brackets change position to mimic the natural cross-sectional change of the boom. Parallel to this cross-sectional deployment, bolts integrated into the green rectangular frames lock the boom spool inside the outer mechanism body.

Many more details on this concepts like the used actuator as well as the trigger-concept are described in a dedicated paper[7].

C. Concept Discussion

Both concepts have their pros and cons that are listed below in Table 1.

The choice of the optimal concept for a dedicated deployable application depends on the boundary conditions of this scenario. *Concept A* seams to be less complex and universal while *Concept B* might be suitable for some mechanically very performance demanding application that can accept the added complexity and the blocked volume in the boom spool cavity. Applications that could fit those properties are instrument booms, solar arrays or solar sails.

On the other hand, *Concept B* does not require the large floating core unit that also needs to be located at minimal distance to the boom spool to allow the boom to open up sufficiently.

IV. Devices under Test

The figures Fig. 7 and Fig. 8 show the actual hardware tested. For both demonstrators the structural components are mainly 3d-printed but some core components are machined out of aluminum and steel. Standard parts like motors, sensors, ball bearings, springs, screws and nuts are used as well.

Concept A is driven by a simple brushed DC gear motor. The deployment and stowage of the boom can be realized by simply changing the motor direction.

Concept B is driven by an advanced brushless DC gear motor and is also equipped with a space-grade launch lock

	Concept A	*Concept B*
Pros	High bending stiffness and strength during deployment and in deployed state.	Very High bending stiffness and strength in deployed state.
	Boom spool cavity empty and thus usable by other components.	Minimum friction at guiding surfaces.
	Simple concepts with passive mechanisms.	Compact design
	Boom can be retracted again after full deployment.	
Cons	Increased friction between boom and guiding surfaces requiring higher motor torque budget.	Additional complex mechanisms.
	Not exploiting the fully capability of the booms stiffness and strength.	Boom spool cavity is filled with mechanisms and is not available for other components.
	large volume to accommodate floating core interface	Root deployment is a one-shot mechanisms that would not allow for an on orbit retraction.

Table 1 Comparison of *Concept A* and *Concept B*

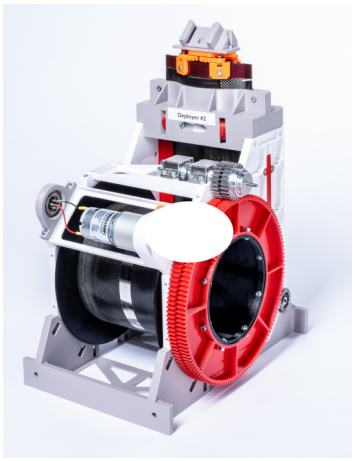

Fig. 7 Boom deployment mechanism utilizing *Concept A*

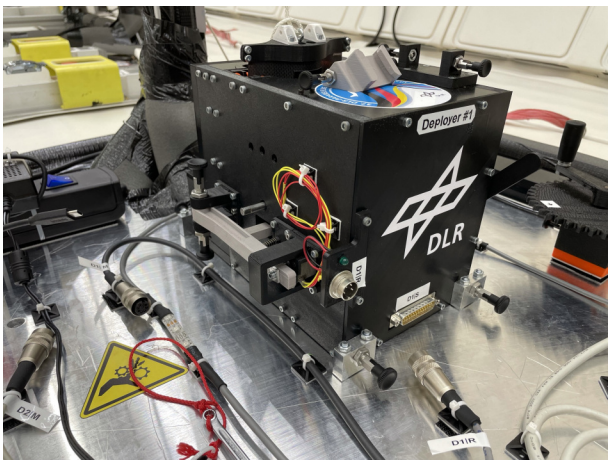

Fig. 8 Boom deployment mechanism utilizing *Concept B*

actuator. This prototype was furthermore equipped with a force sensor, a rotary encoder and some end-stop switches. As the mechanism inside the boom spool requires a manual reset by an operator, only the deployment of this concept was considered a test while the stowing was defined to be a refurbishment activity.

V. Test Objectives

The basic motivation of the test was to demonstrate the deployment and stowing of both concepts in relevant environment to help to further mature both designs, increase the TRL and pave the way for future in orbit tests.

A secondary objective was a brief modal survey to characterize their bending stiffness. For *Concept B* those tests were conducted each before and after triggering the boom root cross section deployment kinematic. For *Concept A* only the deployed configuration has been tested.

Thus the following objectives were defined:

- *Concept A*

  ObjA.1: Demonstrate motorized deployment of the boom and observe the proper behavior of the deployment

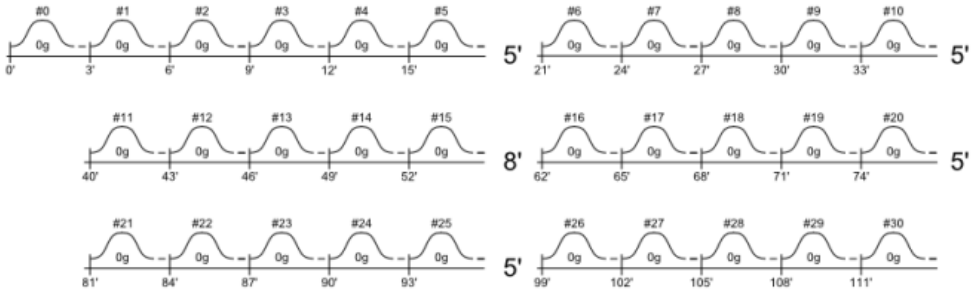

Fig. 9 Plan for a normal flight day (Source: NOVESPACE)

mechanism.

ObjA.2: Demonstrate motorized direction switch from deployment to retraction of the boom and observe the proper behavior of the deployment mechanism.

ObjA.3 Demonstrate motorized retraction of the boom and observe the proper behavior of the deployment mechanism.

ObjA.4 Validate bending stiffness x and y direction at fully deployed state by manually excited swing-out tests.

- *Concept B*

  ObjB.1 Demonstrate motorized deployment of the boom and observe the proper behavior of the deployment mechanism

  ObjB.2 Demonstrate electrically triggered the boom root deployment and observe the proper behavior of the mechanism

  ObjB.3 Validate bending stiffness x and y direction by manually excited swing-out tests for longitudinal fully deployed boom without deployed boom root.

  ObjB.4 Validate bending stiffness x and y direction by manually excited swing-out tests for longitudinal fully deployed boom with deployed boom root.

VI. Test Environment

Both prototypes where tested within DLR's 37th parabolic flight campaign in 2021. As usual this flight was operated by the french company NOVESPACE[§]. DLR usually conducts 1 or 2 campaigns per year. For each campaign the 20m x 5m test area is divided into about 14 smaller test areas for the same number of individual tests. In this configuration, the aircraft then completes one flight each with 30 test parabolas on three consecutive days providing each group of scientists with 90 parabolas.

Fig. 9 shows the flight plan for a normal flight day. Actually, the day consists of 31 parabolas, whereby the first parabola (parabola #0) is intended for the acclimatisation of the experiment operators and the pilots and no experiments are conducted in it. The experiments start from parabola #1. There are 6 sets with 5 parabolas each and breaks of about 90 seconds between the individual parabolas. Between each set of 5 there are longer breaks between 5 and 8 minutes. During the breaks, the machine is in cruise flight and the operators can prepare their experiments for the next set.

Fig. 10 shows the original sensor data of two consecutive parabolas and the short break in between. The black line represents the course of the flight altitude, the blue curve the g-level. It The altitude is varying between 6000m in cruise flight and 8500m at the top of the parabola.

Each maneuver is split into 4 phases:

1) Pull-Up from second 0 till 20: Aircraft is pulled up to follow the first lower part of the parabola until an upward pitch of about 45° is met. Increased g-levels up to 1.8g are present within the aircraft.
2) Phase of weightlessness from second 22 till 45: Aircraft is following the upper part of the parabola.

[§] www.airzerog.com

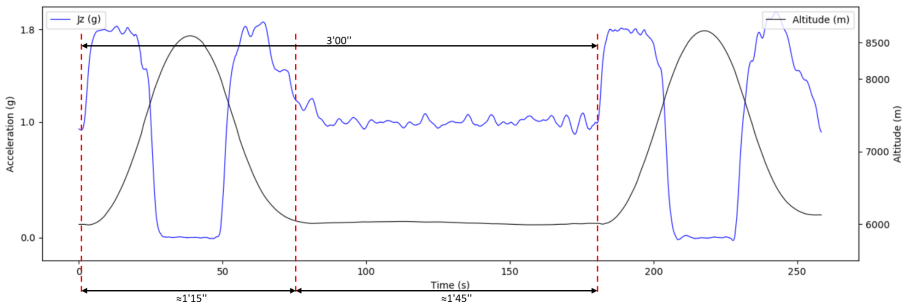

Fig. 10 Flight altitude and g-level during and between parabola maneuver (Source: NOVESPACE)

Fig. 11 Entire crew of experiment operators

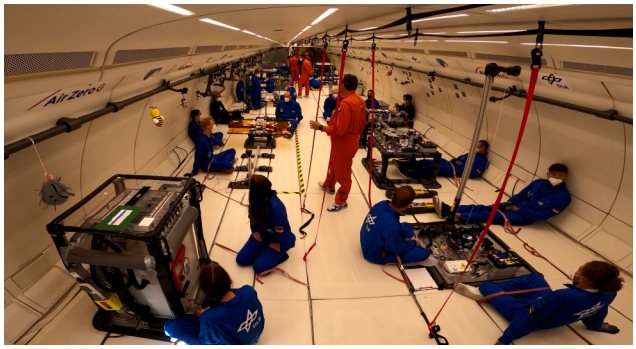

Fig. 12 Impression of the cabin in flight

3) Pull-Out from second 47 till 75: Aircraft is pulled out of its 45° dive until it is back to 0° pitch. Increased g-levels up to 1.8g are present again within the aircraft.
4) Cruise flight for about 90 seconds.

Because the three parallel acting pilots have to stabilize the g-level in all three spacial direction manually, the first 2 to 4 seconds of phase 2 can not be used for sensitive experiments. Therefore, each parabola provides between 18 and 20 seconds of proper so-called *micro-gravity*. During this time span the following requirement are met:

- vertical axis: $|a_z| < 0.02g$
- longitudinal axis: $|a_x| < 0.01g$
- lateral axis: $|a_y| < 0.01g$

Particularly because of the one 16m long and the one smaller experiment of a DLR-NASA cooperation project, it was decided to include an additional fourth day in the flight plan. This day was reserved only for experiments of this technology. In total, there were 5 experiments on board on this flight day, all of which had to do with deployable space structures. Three of them tested boom deployment mechanisms or their applications [6, 8], one demonstrated a new bio-inspired structurally supported deployable membrane [9] and one was dedicated to post-test of tape hinges used on the DLR satellite Eu:CROPIS for solar array deployment.

Fig. 11 shows the entire team that operated the 5 experiments. In total, 18 operators were needed to carry out the experiments. The majority were contributed by DLR. Due to the aforementioned DLR-NASA cooperation, two NASA partners were joining the flight. In the spirit of promoting young talent, 3 of the 16 DLR operators were former or active students who were involved in the rack designs or integration of one experiment.

Fig. 12 shows a single extracted frame of one of the cameras that were filming the entire flight. The experiment described here as well as its 3 operators can be seen in the lower right corner of this picture.

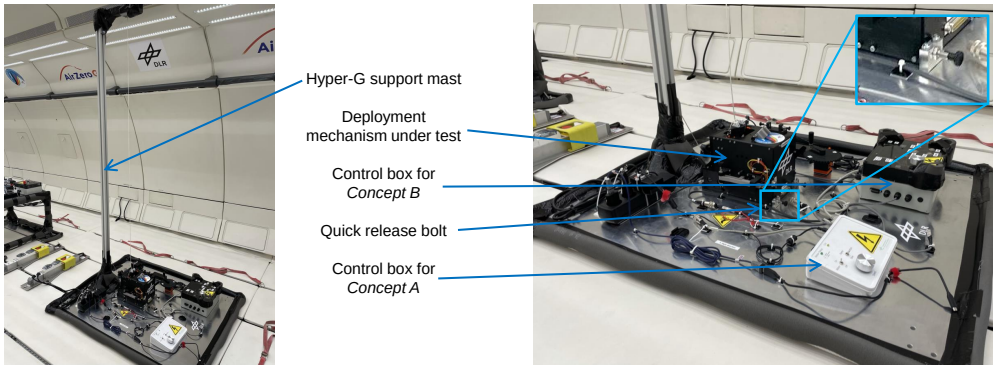

Fig. 13 Labeled setup of the test rack in the aircraft.

VII. Test Setup

A. Mechanical Setup and Accommodation

Fig. 13 shows the setup of the test as finally installed in the test aircraft with labeled parts. The entire setup is bolted onto a 10mm thick solid aluminum plate that is bolted to the aircraft seat rails with 4 massive screws (hidden under the grey foam tubing at the base plate edges). In this figure the *Concept B* deployment mechanisms is installed. However, realized by a quick release attachment concept relying on 4 locking-bolts as well as proper electric connectors, the mechanisms of both concepts can be swapped in a few seconds. Both concepts provide identical adapters at the boom tip to accommodate a battery driven camera that should on one hand document the experiment from this perspective and on the other hand provide a constant tip mass for the performed vibration tests.

One very prominent part of the setup is the support mast. It is provided with some pulleys and a thin rope that is used as safety rope to secure the fully or partially deployed boom during the 1.8g phases that take place between the 0g phase. One end of the rope is attached to the boom tip. The other end is basically free and can be controlled by hand by one of the operators. Between the individual parabolas this free end is secured in a rope clamp (sailing equipment). The

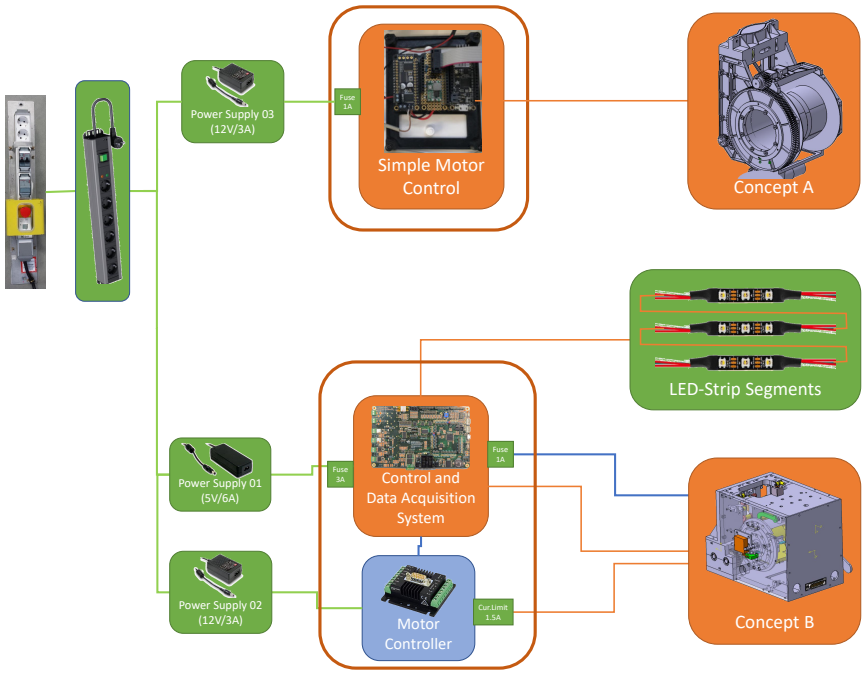

Fig. 14 Schematic of the test setup electronics.

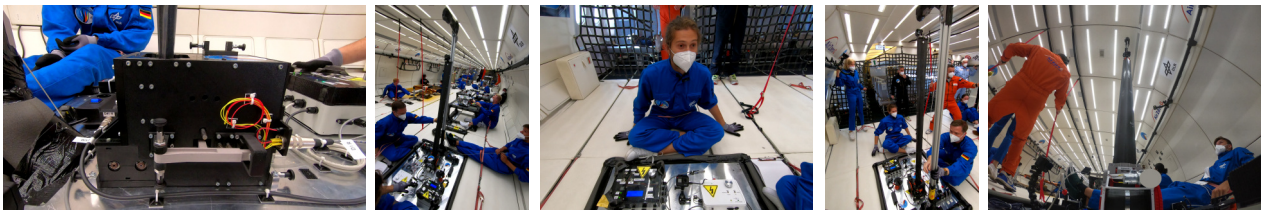

(a) Cam #1 (b) Cam #2 (c) Cam #3 (d) Cam #4 (e) Cam #5

Fig. 15 Field of view from all five camera

rope was always well tensioned during all non-0g phases but had sufficient slack during the actual testing at 0g.

B. Electric Setup

Fig. 14 show the complex electric schematic that was required to operate the setup. Each deployment mechanism is run by its own custom electronics box. Given by the fact that the *Concept B* unit was equipped with more sensors and actuators, the electronics of this model were also more complex. It could deploy the system automatically, stop once the longitudinal deployment is finished and could also trigger the boom root deployment. In parallel it records all relevant sensor data as well as system variables and a time stamp from an included RTC (real time clock) to an included memory card. This box also controlled three short pieces of a LED strip that were used to later synchronize the obtained data of the rack-electronics with the camera footage of the observing cameras.

In total 2 cameras were installed at the handrails of the aircraft to observe the entire experiment (Fig. 15b and 15d). Two cameras were attached to the experiment base plate. One of them focused on the trigger actuator for the boom root deployment (Fig. 15a). The second was looking up to the boom tip in order to have a good view on the shaking boom tip during the modal tests (Fig. 15e). The fifth camera is the one attached to the boom tip (Fig. 15c).

VIII. Test Plan

Table 2 provides insight into the test plan for the flight day. The 30 test parabolas were equally split between both concepts.

A. Concept B

Concept B used the first 3 sets of 5 to basically repeat the same test plan three times. The mast was deployed along 3 parabolas in order to test with representative deployment speed.

In the first part of the fourth parabola of each set, the mast tip of the fully deployed mast was deflected by one of the operators manually and then released. The mast was then given a few seconds to complete up to 5 complete oscillation periods. Depending on the stiffness, between 2 and 6 of these swing-out tests could be performed in a row in one parabola. The operator regularly changed the direction between the individual excitations so that the decay behavior could be observed in the x and y direction [¶].

Towards the end of this parabola, the other operator then triggered the deployment of the mast root via the control box. As this sub-mechanism was driven by a relatively powerful pre-tensioned spring, it was completed in a few fractions of a second.

In contrast to *Concept A* the deployment is not stopped by the operator but by the electronics that sensed the end of the longitudinal deployment by an end stop within the deployment mechanism. For this concept it is very vital to stop the deployment at the very correct spot. That means that the boom need to be fully un-spooled from the spool and the spool need to be in the correct angular orientation, with respect to the mechanism outer walls, in order to activate the boom root deployment sub-mechanism without damaging the boom and/or jamming the mechanism.

The last parabola of each set was used to repeat the swing-out tests with deployed root mechanism. Again several swing-out tests could be carried out in different directions.

At the end of each of the first three sets the demonstrator was refurbished to its initial, stowed state. Therefore, the boom root deployment mechanism was reset with an external tool operated by one operator. The triggering release nut

[¶]please refer to Fig. 2 on page 2 for local boom axis definition

Parabola	*Concept under Test*	*Test Description*
#1	Concept B	Deployment up to 33% length
#2	Concept B	Deployment up to 66% length
#3	Concept B	Deployment up to full length
#4	Concept B	Vibration decay tests followed by triggering of boom root deployment
#5	Concept B	Vibration decay tests after boom root deployment
#6 .. #10	Concept B	repeating test of parabola #1 to #5
#11 .. #15	Concept B	repeating test of parabola #1 to #5
#16	Concept A	Deployment up to 20% length
#17	Concept A	Deployment up to 50% length
#18	Concept A	Deployment up to 80% length
#19	Concept A	Deployment up to full length
#20	Concept A	Vibration decay tests
#21	Concept A	Deployment up to 50% length
#22	Concept A	Deployment up to full length
#23	Concept A	Direction switch from deploy to stow and stow 5cm
#24	Concept A	Stowing down to 50% length
#25	Concept A	Stowing down to fully stowed
#26 .. #30	Concept B	repeating test of parabola #16 to #20

Table 2 Test plan

launch lock actuator is based on a non-destructive SMA (Shape Memory Alloy) principle. Thus it could be reset very easily but simply pressing the released nut back into its locking cavity. The retraction of the boom was done with an external, manually operated tool.

B. Concept A

As *Concept A* was less complex and also able to retract the boom itself, the test plan looks a bit different. With no boom root deployment necessary, the deployment was distributed across 4 parabolas for 2 out of 3 test sets. The fifth parabola was than used for swing-out tests. The refurbishment for the next set was done simply by reversing the drive direction of the motor. As *Concept A* provides a good amount of stiffness in all deployment phases, this could be done under 1g cruise flight without any additional support of the boom tip.

In the fifth test set (parabola #21 to #25) the deployment should be done with doubled speed in order to deploy the mast within two parabolas. The third parabola of this set was used to demonstrate the direction switch from deployment to stowage under weightlessness. During the last two parabolas the boom was retracted back to the stowed position.

IX. Test Results

A. Concept A

1. Proper mechanism operation

The deployment mechanism utilizing *Concept A* was performing absolutely flawless (see Fig. 16). The three deployment tests as well as the one retraction test in microgravity were running smooth no matter if the motor was run faster or slower. Although loaded with a tip mass of 300 gram the boom was never close to buckling even under 1g or 1.8g load.

After the flight, the mast was thoroughly checked for possible damage, but also for traces of grinding or color changes. No changes could be detected.

During review of the camera footage it was observed that one operator was overloading the boom unintentionally while manually deflecting it in boom x-direction for the swing-out test (see Fig. 17). The footage shows how a buckle formed at the compressive loaded boom flange during operator manipulation. Once the operator releases the boom to

(a) fully stowed (prior to parabola #16)

(b) fully deployed (during parabola #20)

Fig. 16 *Concept A* in flight

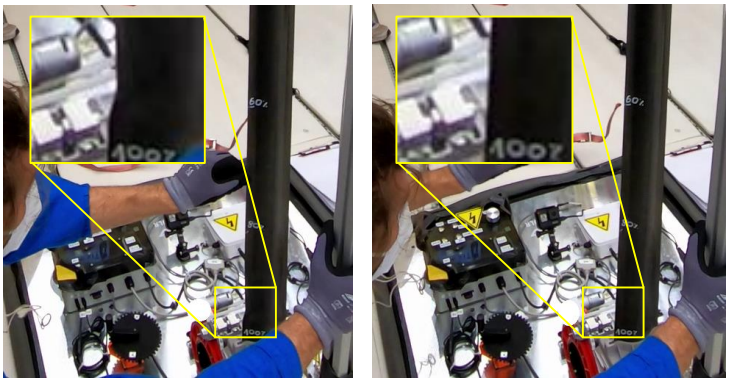

Fig. 17 Boom forms buckle at boom flange while overloaded by operator (left). Buckle pops out without damage after release by operator (right).

start the swing-out, the buckle popped out by it self. This unintended overload also demonstrates the robustness of the concept.

2. Swing-Out tests

The swing-out test were analyzed using the free image analysis software *Tracker*[‖]. The software is able to examine videos and automatically track points of interest. These points do not have to be special targets but only have to stand out clearly from the background and not move too much between two video-frames.

In the course of initial pre-processing of the various camera recordings, a combined video was created showing three different scenes on one screen. All partial videos were synchronized with the audio tracks of the individual segments. The clearly audible announcements of the pilot during the flight were used for this.

Fig. 18 and 19 shows two output of the analysis of this combined video with the *Tracker* software. In both figures the same mentioned video is used as source but the software was advised to track the movements of different features of the video (marked with a yellow circle).

Both analyzes show a good vibration decay sequence between 11s and 13.5s. For both spots the movements in

[‖] https://physlets.org/tracker/

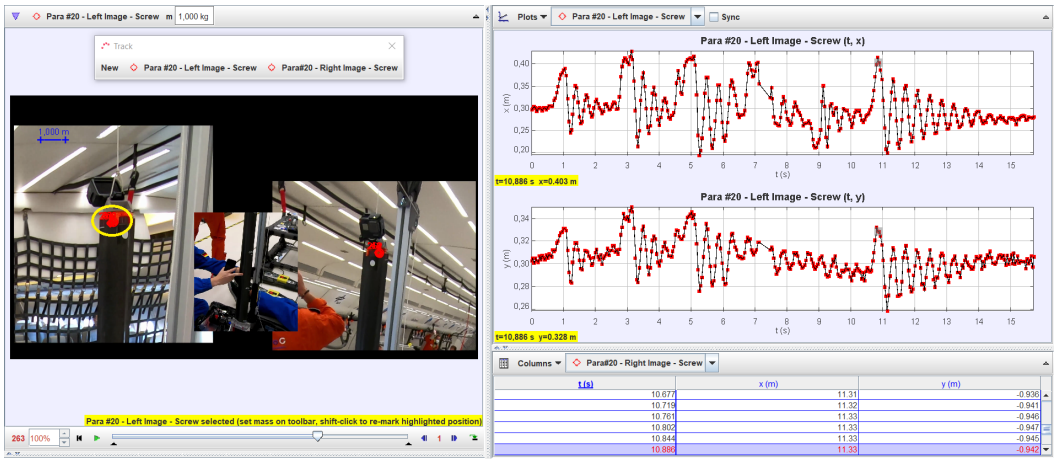

Fig. 18 Video analysis of partial footage of Cam #4 during parabola #20

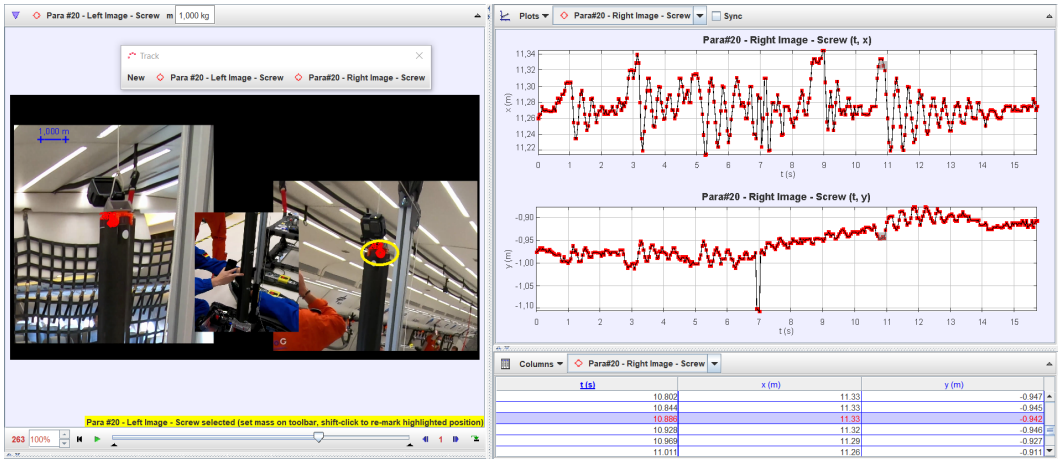

Fig. 19 Video analysis of partial footage of Cam #2 during parabola #20

horizontal image direction (x-direction) was used for further calculation.

The vibration frequency was derived by selecting a potentially high number of clearly identifiable vibration periods. By determining the time span of this sequence $T_{decay,n}$ and the number of full periods n_{decay} one can calculate the resulting frequency f_A by Eq. (1).

$$f_A = \frac{n_{decay}}{T_{decay,n}} \tag{1}$$

For the tracking of Cam #4 a frequency of $f_{A|Cam4} = 2.66Hz$ and for Cam #2 a frequency of $f_{A|Cam2} = 2.57Hz$ have been calculated.

As described in Chapter VIII, the swing-out test should be performed multiple times and alternating between both boom bending directions. However, it turned out that the bending stiffness around the boom y-axis** is significantly increased in contrast to the stiffness around the x-axis. While this is a good point for later applications it led to issues with the used test method for test around the boom y-axis. The boom tip could not be deflected by a noticeable distance without overloading the boom and cause local buckling (see again Fig. 17). When loaded properly the resulting vibration was damped strongly and couples into the x-bending vibration after 2 to 3 full oscillations.

The best observed bending around the y-axis can be seen in Fig. 18 between $9.1s$ and $10.4s$. The characteristic is too unclean and the number of oscillations is too small to derive a frequency from this data.

**please refer to Fig. 2 on page 2

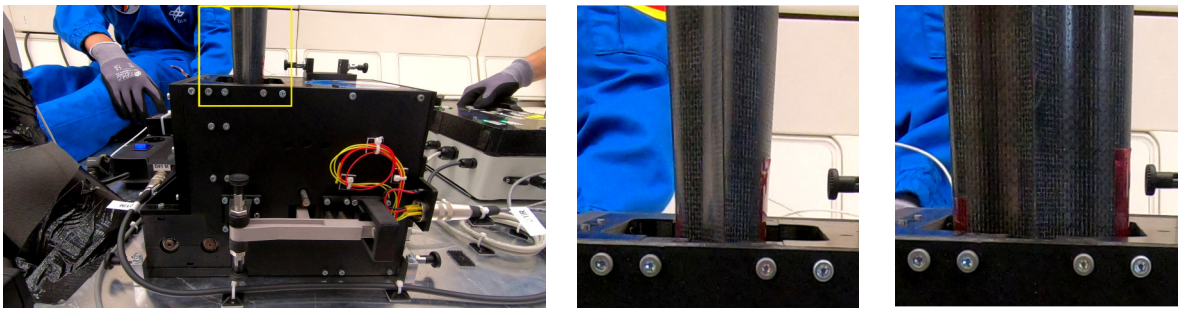

(a) Total field for view of Cam #1 **(b) Enlarged view on the boom before root deployment** **(c) Enlarged view on the boom after root deployment**

Fig. 20 Boom root deployment in parabola #4

B. Concept B

1. Proper mechanism operation

On first evaluation, the deployment mechanism utilizing *Concept B* was performing flawless as well. The three deployment tests in microgravity were performed as planned. This is true for both the longitudinal deployment including automatic stop and the boom root deployment.

The effect of the boom root deployment is visualized in Fig. 20 from the perspective of Cam #1. Fig. 20a shows an overview frame that was made with a fully deployed boom but un-triggered boom root deployment mechanism. Fig. 20b shows an enlarged section of the identical image shown in Fig. 20a. Finally, Fig. 20c shows the same section after the boom root has been unfolded. It is obvious that the boom is much wider after the triggering of this mechanisms. Moreover, one can see that the cross-section no longer opens up further throughout the length, but is the same size everywhere.

Regarding the general appearance of the deployment it needs to be stated that the reduced support of the boom *before* the boom root deployment led to a significant decrease in bending stiffness. The deployed portion of the boom was swiveling in positive and negative y-directions by about ±5°. During deployment and during the swing-out tests such panning also happened spontaneously while there was not obvious reason for this at this point. It was later understood that this reaction was caused by a short inaccuracy in the micro-g environment that was effecting a relative heavy tip load that was mounted to a boom with limited bending stiffness in its root interface.

While this could be accepted for a later application in space with a true 0g environment it could cause a severe risk for the boom root deployment. If the mast is not well aligned it the moment the root deployment is triggered, the root deployment could jam or - if this sub-mechanism is actuated with enough force - even damage the boom itself. On the other hand, so far the inner boom deployment mechanism is driven by a preloaded spring. When substituting this actuator with a gear motor a more gentle and possibly even reversible new concept could result.

2. Swing-Out tests

Fig. 21 and Fig.22 show results from the conducted analysis of *Concept B* related footage. Both Figures show data from test with excitation deflections in y-direction that initiate vibrations around the boom x-axis. This axis is the one that is most effected from the stiffness reduction in the transition zone (see again Fig. 3 on page 2). This is visualized well in Fig. 21 as the boom tip never completed one full oscillation but only pan a bit back and forth to finally come to a stop at a random angle. Some rough estimation using the first half oscillations would results in oscillation periods about $3.0s$ to $3.5s$ and derived frequencies between $0.26Hz$ and $0.33Hz$. However, this could be only give an impression of the order of magnitude and can not considered to be a well-obtained result.

Once the boom root is deployed (see Fig. 22) the behavior changes significantly. Clear damped vibrations can be recognized for the three graphs.

Fig. 23 and Fig. 24 show the same results for tests with excitation deflections in x-direction that initiate vibrations around the boom y-axis. In contrast to the analysis in the other direction a clear vibration pattern forms in the graphs even for the mechanism without deployed boom root (see Fig. 23). This results from the fact that the weakening of the bending stiffness is only true for bending around the x-axis. The bending stiffness around the y-axis is theoretically

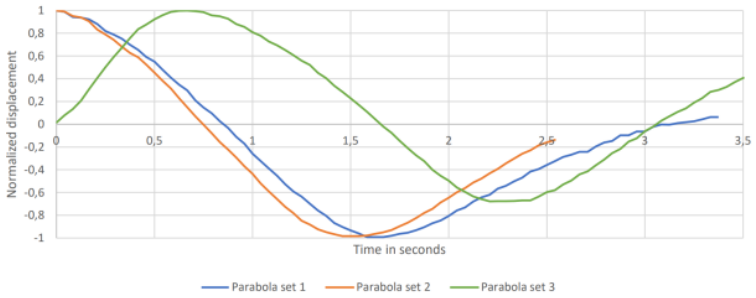

Fig. 21 ***Concept B*** **tip deflection due to manual excitation before boom root actuation (bending aroud x-axis)[10]**

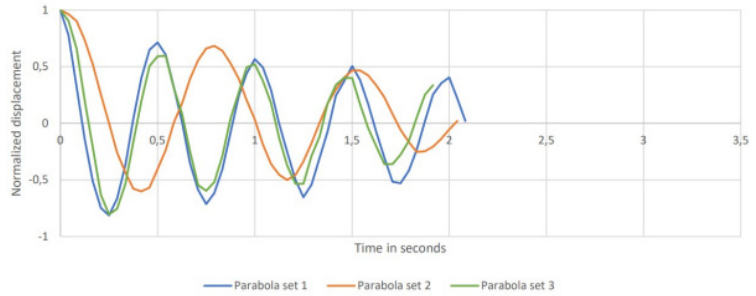

Fig. 22 ***Concept B*** **tip deflection due to manual excitation after boom root actuation (bending aroud x-axis)[10]**

even higher in this region as the boom cross section is wider in x-direction. However, due to the reduced stiffness in y-direction the vibrations in x-direction are strongly coupled with movements in y direction. Therefore, only the first parabola set (parabola #4) in Fig. 23 could be analyzed more in detail. The average period is about $0.64s$ resulting in a oscillation frequency of about $1.56Hz$.

Fig. 24 shows again a clear vibration characteristic and could be used to obtain vibration frequencies.

Table 3 compiles all swing-out test results for *Concept B* . All values written in round brackets could be only obtained by picking one full or even a half oscillation period and are therefore not considered reliable.

However, when comparing the reliable value, $f_{B|stiff|Mx}$ obtained in parabola #10 attracts interest. Luckily, the footage of Cam #1 could provide insight into this massive drop in stiffness. Fig. 25 compiles three similar images of this camera taken in each of the three sets after the boom root has been deployed. The two yellow dashed lines shall help to see the issue that is highlighted with the red ellipse. The root deployment at set 2 was initiated but not carried out to its full extend. While the difference in deployed width looks minor, it also suggest that the four boom root interface brackets (please refer again to Fig. 6b on page 4) haven't reached their final positions and are therefore not fully locked into the spool. Due to the kinematic coupling of the root deployment and the locking of the spool in the outer structure, it is also probable that the spool is not firmly locked into the mechanisms side walls.

X. Conclusion

All previously defined test objectives (see Chapter V) have been met. Both concepts demonstrated their operation under relevant environment and the test campaign was assessed to be a full success.

Parabolas	$f_{B\|weak\|Mx}$	$f_{B\|weak\|My}$	$f_{B\|stiff\|Mx}$	$f_{B\|stiff\|My}$
#4, #5 (Set 1)	$(0.26Hz)$	$1.49Hz$	$2.1Hz$	$1.9Hz$
#9, #10 (Set 2)	$(0.33Hz)$	$(1.7Hz)$	$1.2Hz$	$1.7Hz$
#14, #15 (Set 3)	$(0.26Hz)$	$(1.8Hz)$	$2.1Hz$	$1.8Hz$

Table 3 Oscillation frequencies for *Concept B*

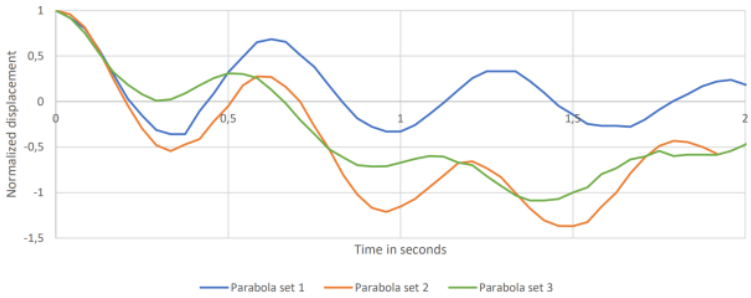

Fig. 23 ***Concept B*** **tip deflection due to manual excitation before boom root actuation (bending aroud y-axis)[10]**

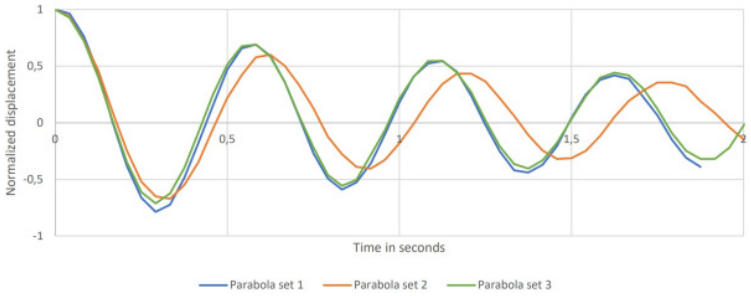

Fig. 24 ***Concept B*** **tip deflection due to manual excitation after boom root actuation (bending aroud y-axis)[10]**

A. Concept comparison

Comparing both concepts, the prototype of *Concept A* was performing a bit better than *Concept B* . The expected increased stiffness of *Concept B* over *Concept A* could not be be confirmed. *Concept A* oscillated at about $2.6Hz$ while *Concept B* could achieve $2.1Hz$. *Concept B* showed however the potential of its boom root deployment that increased the oscillation frequency of the boom by an order of magnitude once the root deployment was triggered.

One minor deployment failure was observed for *Concept B* while *Concept A* was operating without any problems. The very same *Concept A* mechanism was equipped with a $4.3m$ long boom in 2022. It preformed about 40-50 deployments and retractions under 1g (again with a camera at the tip, no gravity compensation) at the ILA BERLIN Expo and the SPACE TECH EXPO Bremen.

Nevertheless, the authors of this paper are convinced that the basic principles of *Concept B* will be able to push the stiffness much higher as observed with the here presented prototype. Typically, the use of plastic parts is a valid approach for deployment mechanism prototypes and for the evaluation of the deployment it has served its purpose within this test series. However, when it comes to stiffness measurements, this material exchange can no longer be

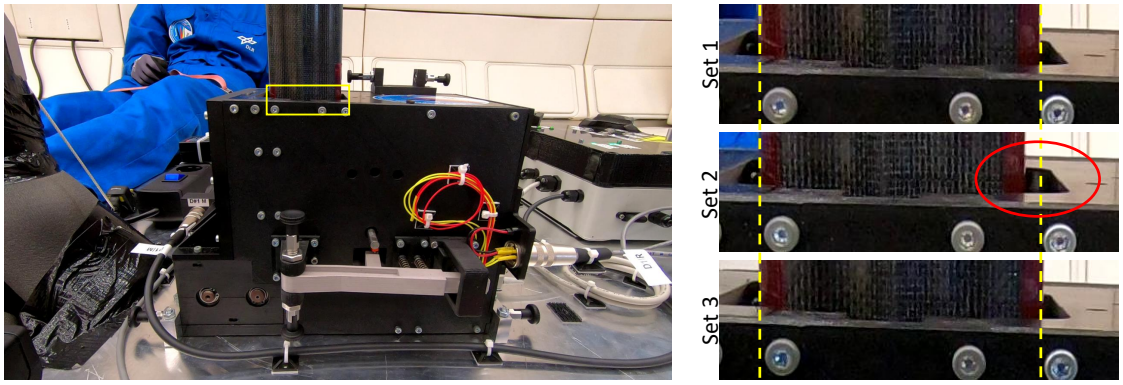

Fig. 25 Deployed boom root of ***Concept B*** **seen by Cam #1 for each of the last parabolas out of the three** ***Concept B*** **test sets (important spot is marked with a red ellipse)**

neglected. Bending loads on the 2m long mast generate large individual force-pairs at the small boom support bracket in the mechanism, which must be absorbed by these small parts and the kinematics behind them. Some parts of these kinematics are still made from plastic in the current prototype. It is expected that a mechanism with stiffer components as well as a play-minimized design will generate a significant increase in stiffness. Thankfully, zero gravity will not be required for such stiffness tests on a new prototype. These tests will be performed in-house with existing test facilities.

B. Lessons learned on 0g testing

As always communicated by the service provider, a parabolic flight does not provide 0g but μ-g (micro-g). This is true for the vertical but also for the longitudinal and lateral aircraft axis. Thus some movements of the deploying or deployed booms were influenced mainly by lateral and longitudinal very small accelerations. Due to the lower bending stiffness, this effect was only observed for *Concept B* .

When performing dynamic tests like fast deployment or modal analysis on large lightweight structures, one other effect needs to be understood: The surrounding air adds a lot of damping to dynamic processes and thereby influences decay times as well as the deployment behavior.

Concluding, parabolic flights provide a good option to test deployable structures in nearly perfect weightlessness. When planning such test one should make sure that the small disturbances in g-level as well as the still present air can be tolerated or compensated.

For a further understanding of tests in this environment, three related papers for the remaining tests at this parabolic flight can be reviewed as well [6, 8, 9].

C. Test setup

As mentioned above, the focus of this test flight was to evaluate the proper operation of both concepts in weightlessness. The swing-out tests that were analyzed by footage analysis were just considered a *low hanging fruit* that could be added easily to the test plan without any increase in test equipment. However, the not fully deployed boom root at parabola #10 may had remained undetected if the values in Table 3 hadn't raised interest.

Concept B also proved that the vertical support mast and the safety rope were a important features of the test setup. Without it, the mast of *Concept B* would has been bend over and severely damaged during the hyper-g phases.

XI. Outlook

The results of the test series have further strengthened our decision to focus on the floating core concept (*Concept A*) for further DLR developments in the field of high strain composite booms. In 2022 the concept was further streamlined to provide a scalable, modular and retractable concept for various deployable applications (see Fig. 26).

Currently, a 4-boom deployment unit for membrane deployment is under development. A first engineering model design showed that it will be able to carry 4 booms up to 7 m length each. The unit will fit the envelope of a 4-unit CubeSat (2x2x1) and should add a mass between 3 to 4 kg to the spacecraft. Once the unit is integrated, combined boom bending and compression tests will be conducted with this mechanisms to finally determine how close the *Floating Core* concepts is to the ideal rigid interface.

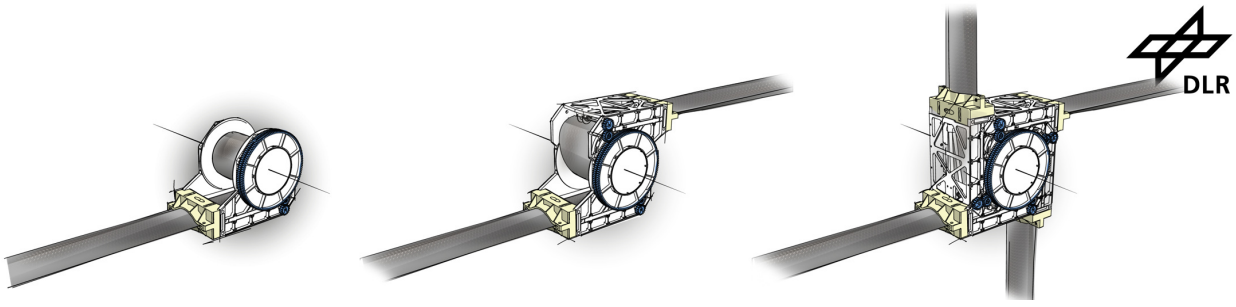

Fig. 26 Modular, retractable boom deployment unit for 1, 2 or 4 booms

Acknowledgments

A significant credit is due to my master student Patrick Henkies, who completely reworked and improved the *Concept B* deployment mechanism for the parabolic flight. He also built and programmed the control electronics from scratch and evaluated the test afterwords and documented it well in his master thesis[10].

Moreover, we would like to thank our institute director Professor Martin Wiedemann, our department head Professor Chrisitan Hühne as well as the team of NOVESPACE for their full support.

References

[1] Straubel, M., "Design and Sizing Method for Deployable Space Antennas," Ph.D. thesis, Otto-von-Guericke-Universität Magdeburg, GERMANY, Sep 2012. URL http://elib.dlr.de/81128/.

[2] Straubel, M., Hillebrandt, M., and Hühne, C., "Evaluation of Different Architectural Concepts for Huge Deployable Solar Arrays for Electric Propelled Space Crafts," *14th European Conference on Spacecraft Structures, Materials and Environmental Testing*, Toulouse, France, 2016.

[3] Hillebrandt, M., Zander, M. E., and Hühne, C., "Apparaturs for Unfolding a Mast," , U.S. Patent 10 717 628, July 21, 2020.

[4] Straubel, M., "Vorrichtung und Verfahren zum entfalten eines aufgerollten länglichen Hohlkörpers," , U.S. Patent Application Publication No. 2020/0324921 A1, October 15, 2020.

[5] Hillebrandt, M., Zander, M. E., and Hühne, C., "Sliding Core Deployment Mechanism for Solar Sails based on Tubular Shell Masts," *Proceedings of 5th International Symposium on Solar Sailing*, 2019. URL https://elib.dlr.de/129630/.

[6] Hillebrandt, M., Meyer, S., Stegmaier, M., Straubel, M., Zander, M. E., and Hühne, C., "Zero-G Deployment Testing of a New Rollable and Retractable Solar Array ," *AIAA SciTech 2023*, National Harbor, MD, USA, 2023.

[7] Straubel, M., and Hühne, C., "CTM Boom Deployment Mechanism with Integrated Boom Root Deployment for Increased Stiffness of the Boom-to-Spacecraft Interface," *European Conference on Spacecraft Structures, Materials and Environmental Testing (ECSSMET 2021)*, 2021. URL https://elib.dlr.de/141680/.

[8] Richter, M., Straubel, M., Zander, M. E., Salazar, J., Chamberlain, M., and Fernandez, J., "Force Application of a Single Boom for a 500-m2-Class Solar Sail," *AIAA SciTech 2023*, National Harbor, MD, USA, 2023.

[9] Zander, M. E., Chamberlain, M., Jost, D., Müller, D., Hagmeister, N., Straubel, M., and Hühne, C., "Design and Testing of the BionicWingSat in a Zero-g Flight Campaign - A 2U-CubeSat with Deployable, Biologically-Inspired Wings ," *AIAA SciTech 2023*, National Harbor, MD, USA, 2023.

[10] Henkies, P., "Design of a GOSSAMER-1 type boom deployment mechanismwith increased boom root stiffness," Master's thesis, University of Applied Sciences Aachen, September 2021.